



Optimization of electroless NiB deposition without stabilizer, based on surface roughness and plating rate



L. Bonin ^{a,*}, C.C. Castro ^b, V. Vitry ^a, A.-L. Hantson ^b, F. Delaunois ^a

^a Metallurgy Lab, UMONS, 20 Place du Parc, 7000 Mons, Belgium

^b Department of Chemical and Biochemical Engineering, UMONS, 20 Place du Parc, 7000 Mons, Belgium

ARTICLE INFO

Article history:

Received 15 January 2018

Received in revised form

25 June 2018

Accepted 26 June 2018

Available online 30 June 2018

Keywords:

Electroless plating

Nickel-boron

Stabilizer

Roughness

Plating rate

Design of experiment

ABSTRACT

The study of the roughness and plating rate of electroless nickel-boron (NiB) coatings produced without stabilizer and the optimization of bath composition based through an experimental design are herein presented. Experiments were carried out using different combinations of a complexing agent, ethylenediamine, and a pH regulator, sodium hydroxide, used in different concentrations. Sodium hydroxide addition showed to improve the plating rate while the incorporation of ethylenediamine affected the roughness of the film in the studied intervals. The optimum combination of bath composition for minimum roughness with maximum deposition rate was derived from the analysis. In order to obtain a film with a thickness between 10.0 and 10.7 μm and a roughness (R_a) between 0.22 and 0.25 μm , both reagents should be combined in the following concentrations: $120.0 < \text{Ethylenediamine (g.L}^{-1}\text{)} < 128.7$ and $151.7 < \text{NaOH (g.L}^{-1}\text{)} < 160.0$. The surface and cross-section morphology of the resulting coatings did not present the typical cauliflower-like structure of electroless nickel-boron due to a different mode of growth. The NiB coatings obtained in this study present 8 wt%. Boron in the composition and a surface hardness of 719 HV_{20} . High corrosion resistance is observed after 240 h of neutral salt spray test.

© 2018 Elsevier B.V. All rights reserved.

1. Introduction

Electroplating, which is commonly described as the conventional electrolytic plating process, is accomplished when metal ions are reduced to the metallic state and deposited as such at the cathode by use of an external electrical source [1,2]. With some similarities but many differences, electroless plating is a chemical reduction process. This process depends upon the catalytic reduction of metallic ions in an aqueous solution containing a reducing agent and the subsequent deposition of the metal without the use of an external source of energy [3–8].

The electroless nickel deposit is formed by the chemical reduction of nickel, which depends on the reducing agent used. Baths reduced by hypophosphite provide a nickel phosphorus coating [9–11] and baths reduced by borohydride [12,13] or aminoborane compounds [14] provide nickel boron alloys. The reaction must be controlled to ensure that the reduction only takes place on the substrate and not on the tanks and other equipment used for plating or in the solution far from the samples. In order to control

this mechanism, additives can be added to the baths. Complexing agents, pH regulators and stabilizers are some of these additives. Stabilizers are the most effective agents used to operate under adequate and stable conditions over extended periods [15–17].

Different bath compositions have been proposed and successfully used to prepare nickel-boron (NiB) coatings for different applications. The deposition rate, properties of the coated components and the structural behavior of the deposits depend mainly on the bath parameters, such as the plating bath constituents, the type and concentration of the reducing agent, complexing agent and stabilizer, the pH, temperature and agitation of the bath [18,19], among others.

Lead has been used as the standard stabilizer for a wide range of industrial electroless nickel processes over the last 30–40 years [20–23]. Lead-based baths are well known and understood, making the process nowadays extremely reliable [16,24–26]. However, over the last years, the emergence of new legislation, aiming towards the improvement of the recyclability of electroless plated products, made the use of lead impracticable and so, new alternatives are required to replace them. In reality, most of the legislation (RoHS [27], ELV [28] and WEEE [29]) allows the use of lead in the plating bath, as long as the deposit presents limited amounts of

* Corresponding author.

E-mail address: luiza.bonin@umons.ac.be (L. Bonin).

lead (about 1000 ppm).

The electroless nickel baths largely applied in the industry in the last years, although purely lead-stabilized, are controlled by specific complexing agents thus ensuring that the lead content in the coating respects the legislations limits [30]. However, as the legislation on environmental issues is progressively strengthening, a higher demand to completely remove lead from electroless nickel is being observed in the metal deposition market. Specifications such as the NSF 61 [29], and some internal corporate rules, for instance the Volvo Black list STD 100-0002 [31], are appealing for completely lead-free electroless nickel processes. Some completely lead-free compositions have been developed for baths reduced by hypophosphite [10,16,31,32], however, only a few works presented options for lead-free baths reduced by borohydride [33,34].

This study presents a completely lead-free plating bath and deposit. The novelty of this work is based on the fact that the achieved bath is completely free of stabilizers. As described before, NiB coatings are traditionally stabilized by toxic heavy metals (like Pb, Tl and Sb). A bath free of stabilizers, without addition of other components, generates an easy recyclability of the coated components. The complexing agent and the pH adjustment, using elements already present in the bath, guarantee the bath stabilization. An experimental design was applied to determine the most suitable bath composition to provide the optimized surface roughness and plating rate in electroless NiB coatings. These two outcomes have been chosen due to different characteristics. The surface roughness provides information about the bath stability: stable baths generate less rough coatings, free of nickel particles adsorbed on the surface of the coating. Additionally, optimization of the plating rate was carried out in order to maintain productivity. As the new bath solution will generate some changes in coating properties, the surface morphology, composition, hardness, tribology and corrosion properties were also addressed in the present work.

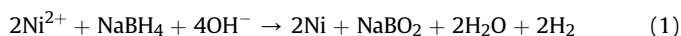
2. Ethylenediamine and pH influence on the bath stability and plating rate

Nickel(II) (Ni(II)) is the most stable oxidation state in the aqueous and non-aqueous solution of nickel. In the absence of strong interacting ligands, in pure water, Ni(II) salts dissolve in water to form the complex $[\text{Ni}(\text{H}_2\text{O})_6]^{2+}$. Then, ethylenediamine (en) (with two donor atoms per molecule) leads to a sequential replacement of the coordinated water molecules and to the formation of mono-, bis- and tris-ligated dications of the general form $[\text{Ni}(\text{en})_n]^{2+}$ ($n = 1-3$) [36,37].

NiB alloys are synthesized by chemical reduction of the nickel ethylenediamine complex. The nickel ethylenediamine complex was found to delay and prevent an abrupt formation and agglomeration of NiB catalysts during the bath preparation [19]. In fact, the metal complex controls the number of free ions that are available participate in the deposition reaction. Additionally, these components prevent the precipitation of alkaline metal salts [18].

Mallory G.O. (2009) [19] presented the relation between the ethylenediamine/nickel molar ratio and the solution stability. When stabilizers are completely removed from the plating solution, higher stabilities are reached for an ethylenediamine/nickel molar ratio between 6 and 7. However, for these values of molar ratio, the plating rate considerably decreases.

In order to avoid low deposition rates, the pH of the solution can be increased [38]. The following reaction (Eq. (1)) displays the reduction of nickel by sodium borohydride [3].



As shown in Eq. (1), the reduction of Ni generates a decrease in

the pH of the solution. So, by increasing the pH of the solution, the tendency for H^+ production increases because of the decrease in H^+ content and, as a result, the deposition rate can be improved. In addition, when nickel ions are reduced, the pH of the solution decreases continuously, generating an increase of the equilibrium potential of the reducing agent couple, thus leading to a diminution of the potential gap between the equilibrium couples of the metal and the reducing agent, all this resulting in a reduction of the deposition rate [18].

The addition of complexing agents in the solution and the pH are relevant factors that affect the nucleation processes of electroless deposits. The pH augmentation probably also influences the composition and microstructure of electroless deposits. However, there is a limited knowledge concerning the effect of complexing agents on the properties of Ni electroless deposits. In the present work, the effect of complexing agents and pH on bath stabilization, deposition rate and coatings properties were studied.

3. Materials and methods

3.1. Sample preparation

The substrate used in these experiments was ST 37-DIN 17100 mild steel with dimensions of $50 \times 25 \times 1 \text{ mm}^3$. A hole of 2 mm in diameter was drilled close to one edge of each piece for convenient handling. Sample surface was polished with emery paper up to 1200 grit to insure uniform surface state between samples. It is important to note that the present study does not consider substrate roughness as an input variable. All samples after different stages of processing and prior to coating should thus have the same roughness. The substrates were prepared for plating by acetone degreasing and etching in a 30 vol % hydrochloric acid solution at room temperature for 3 min.

3.2. Electroless nickel baths

Electroless plating solution (1 L) was prepared on a regulated hot plate with magnetic stirring. Temperature was maintained at $95 \pm 1^\circ\text{C}$ for all samples during the complete plating process. The NiB bath was composed of sodium borohydride, NaBH_4 (99.9% - Acros organics), as reducing agent, in the concentration of 0.602 g L^{-1} , nickel chloride hexahydrate, $\text{NiCl}_2 \cdot 6\text{H}_2\text{O}$ (99% - VWR chemicals), as nickel source, in the concentration of 24 g L^{-1} . Ethylenediamine, $\text{NH}_2\text{-CH}_2\text{-CH}_2\text{-NH}_2$ (99% - VWR chemicals), and sodium hydroxide, NaOH (VWR chemicals), were used as complexing agent and pH regulator, respectively. Different concentrations of these two components were used in the present tests.

In order to establish a basis of comparison with stabilizer-free coatings, electroless nickel-boron samples, stabilized with Pb (NiB-Pb) were prepared following the exact same procedure. The NiB-Pb bath was composed of NaBH_4 (0.602 g L^{-1}), $\text{NiCl}_2 \cdot 6\text{H}_2\text{O}$ (24 g L^{-1}), $\text{NH}_2\text{-CH}_2\text{-CH}_2\text{-NH}$ (59 g L^{-1}), NaOH (39 g L^{-1}) and PbWO_4 (0.021 g L^{-1} - 99.9% - MaTeck GmbH).

3.3. Experimental design for bath optimization

A full factorial design with central point was used to determine the optimal composition of the electroless nickel bath. Two independent factors, also called variables, namely sodium hydroxide and ethylenediamine, were studied. For these two factors, three concentration levels were considered, low (-1), central (0), and high ($+1$), which were respectively, 120, 140 and 160 g L^{-1} (Table 1). The selection of the low and high levels for the factors was performed based on preliminary experiments. A total of ten independent bath combinations was generated by the experimental design

Table 1
Factors and levels used in the full factorial design.

Factors	Low level (-1)	Central level (0)	High level (+1)
Sodium hydroxide (g.L ⁻¹)	120	140	160
Ethylenediamine (g.L ⁻¹)	120	140	160

(Table 2), which were performed randomly by two different operators (all the assays were performed in duplicate). The responses of the experiments considered the maximization of the thickness and the minimization of the roughness of the final coating on the surface of the mild steel.

The experimental design and regression analysis of the experimental data were performed using JMP® 12.2.0 – *The Statistical Discovery Software*. The quality of the fitting model was evaluated by the regression coefficient (R²) and the statistical significance of each factor studied was evaluated by the F-test analysis of variance (ANOVA) for each response variable. The coefficients of the response surface were evaluated using the student t-test.

3.4. Characterization of the electroless NiB coatings

The coating thickness after one hour of deposition was used to determine the effect of the optimal composition on the deposition rate. The coating thickness (μm) was calculated, from the weight gain (W), by the equation below:

$$R = \frac{W \times 10^4}{A \times \rho} \quad (2)$$

where:

W = weight of plated layer (g)

A = plating area (cm²)

ρ = 8.3 g cm⁻² (density of Ni-B alloy by assuming a B-content of approximately 6%).

Roughness measurements (μm) were carried out using a Zeiss 119 Surfcom 1400D-3DF apparatus and the results were analysed using the Zeiss brand software. The presented values are the average of ten measurements.

The surface and cross section morphology of each sample were observed using a Hitachi SU8020 scanning electron microscope. Cross sections were prepared and polished with silicon carbide paper, followed by polishing with diamond paste up to mirror finish and etching with Nital 10%.

The composition of the coatings was determined by Glow Discharge Optical Emission Spectroscopy (GDOES). GDOES analyses were carried out using a HORIBA Scientific GD Profiler 2. The

analysis was carried out in the HORIBA SAS demo lab in Palaiseau (France).

Instrumented indentation micro hardness testing was performed on the samples surface using a standard Vickers four-sided pyramid diamond indenter. The cross section hardness was determined using a Knoop pyramidal diamond point. Hardness tests were conducted on the samples with a load of 20 gf and a holding time of 20 s, for each coating configuration. The results are the average of ten measurements.

A CSEM scratch tester machine with a diamond Rockwell stylus with a radius of 200 μm was used to perform scratch tests. A linearly increasing load from 0 to 150 N was used in all cases, with a scratch velocity of 6.75 mm min⁻¹; the scratch distance was set to be 10 mm. Acoustic emission and friction coefficient were monitored during the experiment. A good notion of the deposit adhesion can be derived with optical analyses on the scratched substrate.

Tribological behavior was investigated using pin-on-disk CSM microtribometer (without lubricant). The samples served as the disks and the counterparts (pins) were 6 mm diameter alumina balls (1400 HV). The sliding speed, sliding distance and normal load, were respectively, 10 cm/s, 100 m and 5 N. The specific wear rate (Ws) was calculated following the European standard EN 1017-13:2008, where the volume wear loss ΔV is divided by the applied load FN and the sliding distance S. The digital optical microscope Hirox KH-8700 was used for the surface analyses. Surface composition after pin-on-disk was analyzed with an Energy-dispersive X-ray Spectroscopy (EDX) - SEM Hitachi SU8020.

Corrosion characterization was performed by Potentiodynamic polarization in 0.1 M NaCl solution with a Bio-logic SP-50 potentiostat. Before the polarization analysis, the open circuit potential (OCP) was recorded for 20 min. Platinum plate and Ag/AgCl (KCl saturated) electrodes were used as counter and reference electrodes, respectively. A potential range of ±0.25 V Vs OCP, at 1 mV/s scan rate, was used.

Additionally, salt spray tests were performed in a Q-FOG Cyclic corrosion tester. Neutral salt spray test was done according to ASTM B117-07. Samples were suspended in a cabinet and exposed to 50 g L⁻¹ ± 5 g L⁻¹ NaCl solution. The air pressure of the atomized saline solution was maintained in the range of 6–8 bar. The tests were conducted for a variety of time periods ranging from 0.5 h to 10 days with intermediate periods of 1 h, 4 h, 8 h and 1, 2, 3, 4, 5, 7 days.

The corroded surfaces after salt spray testing were quantified by image analysis, using the open source image processing and analysis program *ImageJ*. In order to extract and analyse features of a digital image, it is first necessary to identify and separate the different regions. The original images were first transformed in grey-level images. Next, thresholding was used to segment the pixels darker than the threshold value. The *ImageJ* algorithm was

Table 2
Experimental design matrix and response variables values.

	Pattern	Ethylenediamine (g.L ⁻¹)	Sodium Hydroxide (g.L ⁻¹)	Experimental Thickness (μm)	Experimental Roughness (Ra) (μm)	Predicted Thickness (μm)	Predicted Roughness (μm)
1	++	160	160	11.20	0.38	11.75	0.35
2	+ -	160	120	9.50	0.30	9.17	0.35
3	00	140	140	10.50	0.27	9.65	0.28
4	- -	120	120	6.97	0.20	7.54	0.28
5	++	160	160	11.50	0.36	11.75	0.35
6	+ -	160	120	8.70	0.35	9.17	0.35
7	- +	120	160	10.03	0.21	10.13	0.28
8	- +	120	160	10.10	0.22	10.13	0.28
9	- -	120	120	7.30	0.24	7.54	0.28
10	00	140	140	10.70	0.31	9.65	0.28

used along with the semi-automatic thresholding option. This process resulted in a binary file containing only black and white pixels, where the black pixels corresponding to the regions above the threshold value represented the corroded areas. In sequence, the software provided the quantification of the binary images.

4. Results and discussion

The control of electroless nickel coatings can be performed using a large number of factors, such as, bath temperature, concentration of reducing agent, concentration of nickel source, concentration of stabilizer, solution pH, substrate roughness, among others. However, taking into account all these factors in a single study would not be possible, as it would make the size of the design matrix too large. Moreover, the interactions of so many factors when taken into consideration would further complicate the analysis. The aim of this study was to maximize the plating rate, that is, the coating thickness, and minimize the surface roughness of the coating at the same time. Table 2 shows the ten assays generated by the experimental design, combining different concentrations of the complexing agent – ethylenediamine – and the pH regulator – sodium hydroxide –, and the respective experimental and predicted responses for coating thickness and roughness.

Standard least squares analysis was used to evaluate the responses obtained for each assay. Experimental and predicted response values were quite similar (Table 2), showing good correlation factors for thickness ($R^2 = 0.88$) and roughness ($R^2 = 0.92$). The significance of each coefficient was verified by the p -value resulting from the student's t -test (see appendices). The increase of both ethylenediamine and sodium hydroxide concentrations provided an improvement on the coating thickness, although a higher significant effect was verified when increasing the sodium hydroxide concentration (p -value < 0.01). In this context, it is possible to correlate the coating thickness with the pH effect. On the other hand, it was also observed that the decrease of the ethylenediamine reduces significantly the roughness of the coating (p -value < 0.001), meaning that this parameter is more correlated with the complexing mechanism occurring. The statistically significant effects, presenting p -values lower than 0.05 were used to represent the simplified models for the maximization of each response variable, as summarized in Eqs. (3) and (4).

$$\text{Thickness}(\mu\text{m}) = 9.65 + 0.81 \times [\text{Ethylenediamine}] + 1.30 \times [\text{Sodium hydroxide}] \quad (3)$$

$$\text{Roughness}(\mu\text{m}) = 0.284 + 0.065 \times [\text{Ethylenediamine}] \quad (4)$$

In order to provide an optimised mixture of ethylenediamine and sodium hydroxide in the electroless nickel bath, a contour profile was performed (Fig. 1). In this figure, it is possible to observe the variation of the thickness and the roughness of the coating, according concentration range of the two components used. In this context, in order to achieve a thickness range between 10.0 and 10.6 μm and a roughness range between 0.20 and 0.23 μm , the bath should contain amounts of sodium hydroxide and ethylenediamine ranging between 151.7 and 160.0 g L^{-1} and 120.0 and 128.7 g L^{-1} , respectively. In our preliminary studies (results not shown), sodium hydroxide concentrations higher than 160.0 g L^{-1} resulted in the precipitation of nickel hydroxide in the bath which leads to a decrease of the plating rate (samples with 180 g L^{-1} of sodium hydroxide and 120.0 g L^{-1} of ethylenediamine present a 4.16 μm thickness). Also, for an ethylenediamine concentration lower than 120.0 g L^{-1} the bath was not sufficiently stabilized, and so, some

colloidal nickel was formed, increasing the roughness of the coating (samples with 160.0 g L^{-1} of sodium hydroxide and 100.0 g L^{-1} of ethylenediamine presented a 0.32 μm roughness).

The final coating that resulted from the optimised electroless nickel bath, containing 160.0 g L^{-1} of ethylenediamine and 120.0 g L^{-1} of sodium hydroxide, was afterwards characterised in terms of morphology, chemical profile, hardness, scratching and corrosion resistance.

4.1. Morphological properties of the NiB coatings

The morphological properties of NiB coatings produced by the optimised bath mixture composition (without stabilizer, with increased complexing agent concentration and higher pH) are presented in this section. The morphological properties of a conventional NiB-Pb coating produced with lead stabilizer are also used as comparison.

SEM micrographs of the electroless NiB deposits produced with the optimized composition are presented in Fig. 2 (a) and (b). In this figure, it is possible to observe the effects of the removal of the stabilizer on the morphology. The NiB coating synthesized without stabilizer revealed a more uniform and smooth surface morphology, Fig. 2(a), and a featureless dense cross section morphology, after etching with Nital 10%, Fig. 2(b). The morphological variations might be explained by modifications of growth mode during the plating process. Heavy metal stabilizers, such as Pb^{2+} , Cd^{2+} , Ti^{1+} , when added to the plating bath, deposit on the active metal surface through displacement reaction. The presence of stabilizers, adsorbed on the substrate, limited the lateral growth of electroless Ni, resulting in a columnar form of deposit [40] (Fig. 2(d)). The absence of stabilizers in the new bath allowed a uniform and dense growth, as no obstacles were created to the lateral growth of Ni, generating a featureless cross section.

The presence of stabilizers was also responsible for the cauliflower-like superficial structure (Fig. 2(c)) in NiB-Pb samples. The stabilizer obstacles generated a columnar growth and consequently, a superficial structure formed by the column tips. Once more, in the case of a bath free of stabilizer, such structure was not observed and a flat surface was detected instead.

In conclusion, compared with the NiB-Pb cross section observation, significant morphologic variations were caused by the absence of stabilizer. The columnar structure was typically observed for electroless NiB-Pb coatings [25,39], while the NiB showed a featureless morphology. The influence of these morphology changes in the coatings composition are addressed in the next sections.

4.2. Profile chemistry

Depth profile chemical analysis, obtained by Glow-discharge optical emission spectroscopy (GDOES), is presented in Fig. 3. The chemistry of the nickel-boron coatings, free of stabilizers, varied during the plating process and the boron content was close to 9.1 wt% at the beginning of deposition. After the first 2 μm , the boron concentration stabilized at values close to 8 wt%. In the case of NiB-Pb, results of depth profile chemical analysis showed that the boron content did not change with time and was close to 6.2 wt %, while the lead content remained around 0.5 wt%. The NiB-Pb bath was optimized for conservation of chemistry, which was not the case of this new bath.

The difference in boron variation between the two coatings, NiB without stabilizer and NiB-Pb, can be explained by presence of the complexing agent which influences the rate of nickel reduction reaction. So, when more complete nickel-ethylenediamine chelates were formed, the kinetics of nickel deposition and consequently

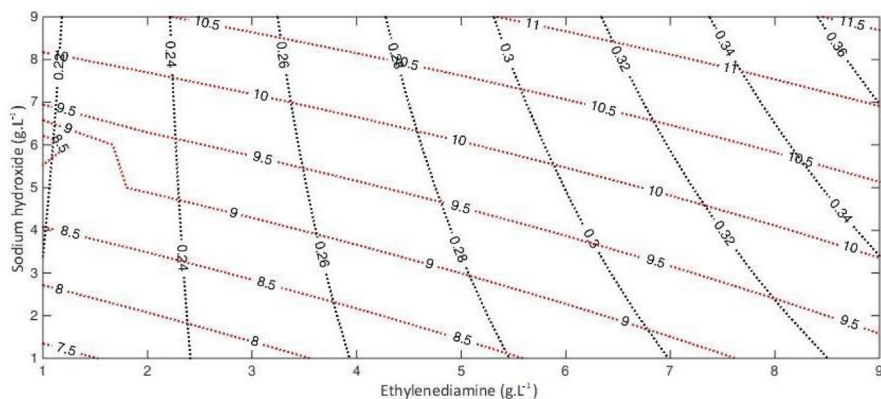


Fig. 1. Contour profile of the thickness (red lines) and the roughness (black lines) of the NiB coatings, according to the concentrations of ethylenediamine and sodium hydroxide in the bath mixture. (For interpretation of the references to colour in this figure legend, the reader is referred to the Web version of this article.)

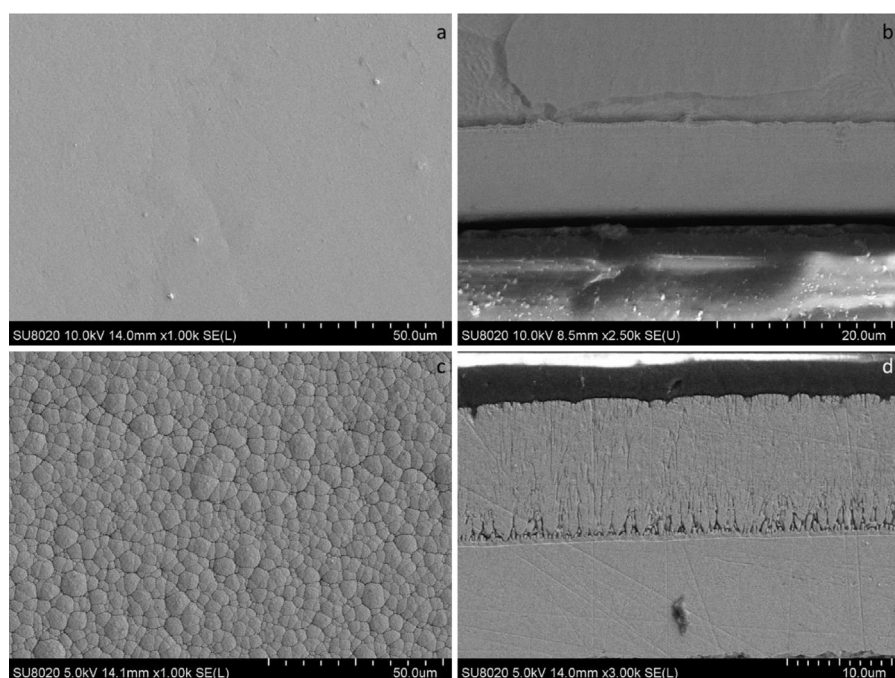


Fig. 2. Morphology of NiB samples: (a) surface morphology of the coated samples and (b) SEM cross section morphology. Morphology of NiB-Pb samples: (c) surface morphology of the coated samples and (d) SEM cross section morphology.

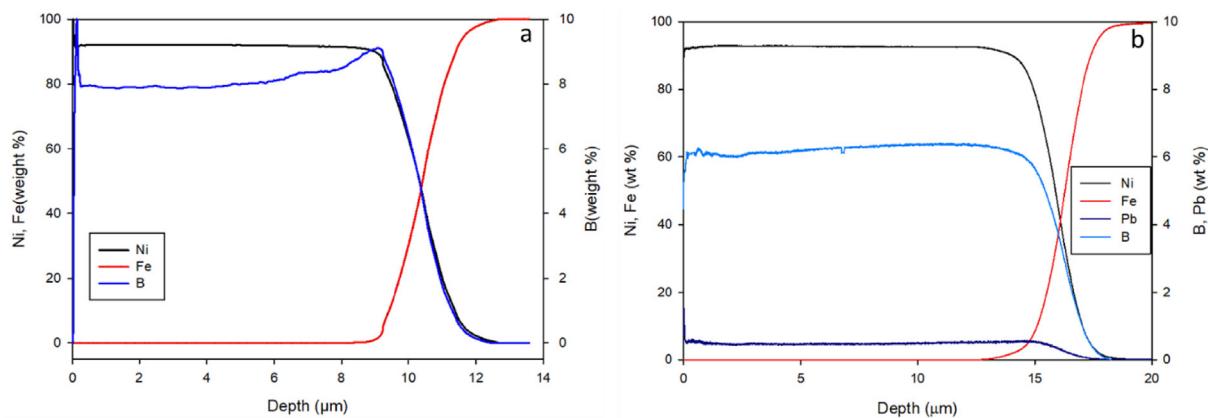


Fig. 3. Depth profile chemical analysis of electroless NiB coatings (a) free of stabilizers and (b) stabilized by lead.

Table 3
Hardness for NiB coating.

	NiB	NiB-Pb
Surface Hardness (hv_{50})	719 ± 13	842 ± 35
Cross section Hardness (hk_{50})	704 ± 25	854 ± 40
Critical load L_c (N)	20	25
Friction coefficient μ	0.48	0.45
Specific wear rate Ws ($\mu\text{m}^2 \cdot \text{N}^{-1}$)	0.81	0.63

the plating rate decreased. However, the borohydride oxidation and the boron reduction reactions were not affected, resulting in a perceptible increase of the total boron content in the coatings.

4.3. Hardness

Surface and cross-section microhardness of the coated systems are presented in Table 3. Nickel-boron coatings are generally considerably harder than nickel-phosphorus. Compared with NiB-Pb coatings [25,40], which presented surface and cross-section hardness of 842 hv_{50} and 854 hk_{50} , respectively, the new coating presented a less impressive hardness, with 719 hv_{50} (surface) and 704 hk_{50} (cross-section). This fact proves that the presence of stabilizer has an influence on the high hardness of NiB-Pb coatings, although the hardness values of stabilizer-free NiB coatings remained superior to those of NiP ones.

4.4. Scratching test

Adhesion of electroless nickel-boron under external solicitations were estimated by scratch test. The method uses an indenter similar to that of a Rockwell hardness tester. In the scratch test, this indenter is used to generate a scratch on the coated system with a determined load and a determined length. In most cases, the load increases continuously with distance and it is possible to observe and identify damage in the coated system for a critical load. The scratched coating surface was analysed by a Hirox KH-8700 Digital Microscope in order to assess the damage features; the distance from the test beginning is used to calculate the critical load.

Fig. 4 shows the scratched coating surface and the detail of the main damaged features, obtained by a combination of acoustic emission and microscopic observations. The first damage was chevron cracks that appeared at 20 N, and transverse semi-circular cracks appeared at 23 N. Complete failure of the coating did not occur for 11 μm thick coatings. In the case of NiB-Pb samples, the first damage induced by scratch testing occurred as chevron cracks from 25 N, then as transverse semi-cracks at 53 N. Moreover, the two damages observed in both deposits were cohesive failures and

a complete failure did not occur for the 15 μm thick coatings.

4.5. Tribology properties

The wear properties for electroless NiB deposits obtained using pin-on-disc apparatus are presented in this section. Tests were realized with a 5 N load, 10 cm s^{-1} of sliding speed and 100 m of sliding distance. After 100 m of test in non-lubricated conditions, the friction coefficient value was about 0.48 for samples without stabilizer. In addition, this friction coefficient was relatively constant from 40 m (Fig. 5). In the case of NiB-Pb, the friction coefficient was generally low (0.45 at 100 m) due to the small effective surface of contact generated by the columnar structure (stabilization was not achieved due to the constant surface area variations). Therefore, when compared with NiB-Pb, NiB presented a superior friction coefficient that reached a steady state earlier. The superior boron concentration of the NiB coatings certainly contribute to the relatively low friction coefficient achieved.

The specific wear rates of these coatings presented in Table 3 are directly related to their hardness. The coatings produced without stabilizer presented an inferior hardness value when compared with the traditional borohydride reduced ones. Consequently, the presented wear behavior of NiB was inferior ($0.63 \mu\text{m}^2 \text{N}^{-1}$) to the one from NiB-Pb ($0.81 \mu\text{m}^2 \text{N}^{-1}$).

The wear mechanisms were determined from observation of the worn surfaces after the pin-on-disk test. Fig. 6 presents the worn surface of the coatings after test with 5 N load. After wear, NiB experienced a superior plastic deformation. Due to the plastic deformation, tribological debris stayed in the wear track and were not present in the neighboring regions. The intermittent load supported by the debris induced a local temperature rise and consequently their oxidation. Debris composition was analyzed by EDX and proved the oxidation of these parts.

The worn surface of the Ni-B coating in Fig. 6(a) shows that the wear grooves were almost completely covered by attached debris. The surface analyses also showed the presence of chevrons in the debris block as a result of its low adhesion with the coating. Adhesion between debris and Ni coatings should not be expected due to their chemical incompatibilities, even though debris were formed from the wear out of the coating, they were constituted of nickel oxidized compounds. For instance, the presence of a layer of debris on the alumina ball can be observed in Fig. 6(b). The oxidation of Ni induces the greater adhesion between the coating debris and Al oxide counter body. In the case of NiB-Pb samples Fig. 6(c), coating exhibited a relatively bright and smooth finishing, with fine abrasion grooves along the sliding direction and a central region with attached debris. The presence of debris in the center of

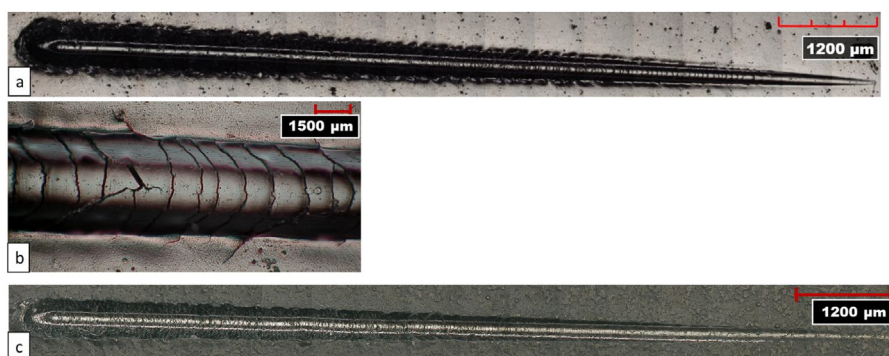


Fig. 4. Electroless NiB free of stabilizer coatings: (a) scratched coating surface; (b) chevron cracks and transverse semi-circular cracks. (c) Electroless NiB-Pb coatings: scratched coating surface.

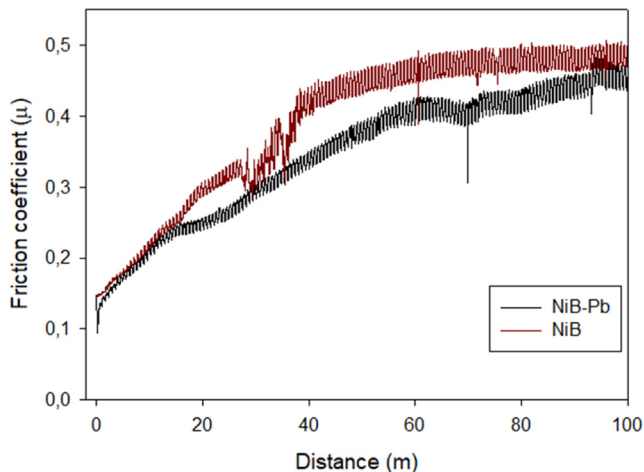


Fig. 5. Friction coefficient evolution of NiB and NiB-Pb samples.

the worn surface can be explained by the columnar texture of these coatings which is able to retain the worn out body. Once gain, due to the chemical affinity, adhesion between the alumina ball and debris can be observed Fig. 6(d).

It is important to observe that delamination and cracking are barely observed for both considered systems. Indeed, composition analyses of the worn surface proved that the wear grooves did not reach the substrates. The overall wear mechanism can be identified as a combination between abrasive wear (alumina ball vs coating) and adhesive wear (alumina ball vs oxidized debris).

4.6. Corrosion

Results of potentiodynamic polarization tests are presented in Fig. 7. The tests were performed on NiB coatings produced using the new composition, on NiB-Pb coatings with the same thickness (10 μm) and on the bare substrate (mild steel), using a 0.1 M NaCl solution. When compared to the bare steel, all the coated samples

presented a better behaviour: a positive shift in the corrosion potential (E_{corr}) and a decrease in the corrosion current densities (I_{corr}). The difference found in polarization behaviour between the coatings and the mild steel suggests that the deposited layers completely cover the substrate and act as barrier coatings [56].

Undoubtedly, differences exist in the surface area of the samples and, in fact, this trend is revealed by the observed differences in the rate of the cathodic reactions; namely, the reduction of oxygen and the evolution of hydrogen (at more negative potentials). In agreement with the surface morphology results, the polarization curves revealed that the higher the surface area the higher the cathodic current densities. Indeed, the NiB-Pb coating, which has the highest surface area (due to the cauliflower-like morphology), presented the highest rates of cathodic reactions, while the NiB coating, with a much smoother surface, presented lower current densities values. Although the coatings presented higher surface area than the bare substrate, they yielded much lower anodic reactions suggesting that, indeed, anodic dissolution was greatly reduced in the case of the coated systems.

Due to the issue of having dissimilar surface areas, a direct comparison of current density values from different coatings is not straightforward. For that reason, when comparing the different systems, only the differences in shape (presence of plateau) of the anodic curves are discussed. Comparing the anodic polarization curves, the shape for the bare steel was similar to the shape for NiB-Pb samples, while the curves for the new NiB coatings presented a less intense increase in the current density. The slower increase for NiB leads to better corrosion resistance and may be explained by the absence of columnar features (intercolumnar zones have been shown to be preferential initiation sites for corrosion on NiB-Pb [41]).

The corrosion potential, E_{corr} , is generally independent of the surface area. The increase in the E_{corr} for the coated systems can then be attributed to the presence of coatings covering the steel surface (Ni is nobler than Fe).

With the aim of further characterizing the corrosion properties, neutral salt spray test was carried out, according to ASTM B117-07. There was no noticeable corrosion pits on the surface of the mild steel-coated samples until 48 h, after which the NiB-Pb samples

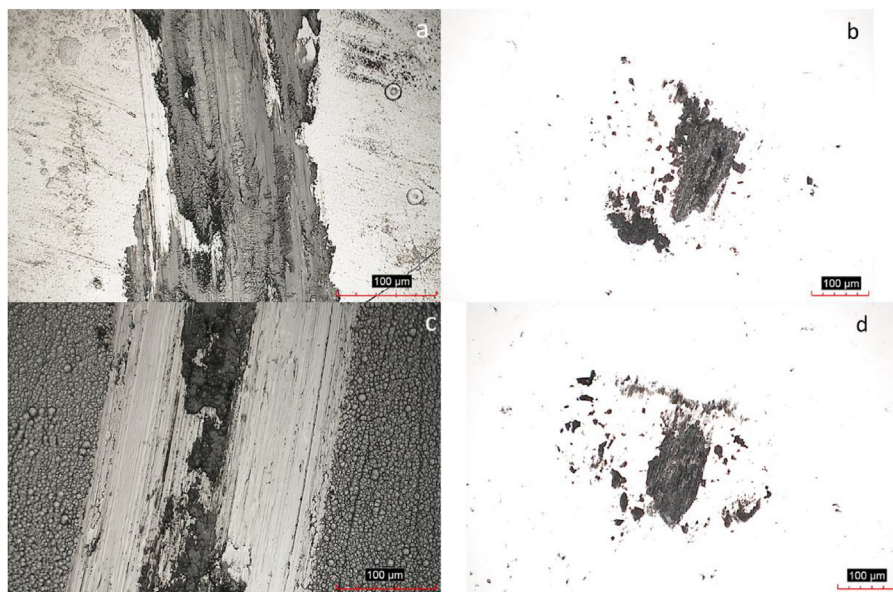


Fig. 6. Optical micrographs of: (a) the wear tracks from electroless NiB free of stabilizer and (b) the surface of alumina balls after the dry sliding friction test. Optical micrographs surface of: (c) the wear tracks from electroless NiB-Pb and (d) the surface of alumina balls after the dry sliding friction test.

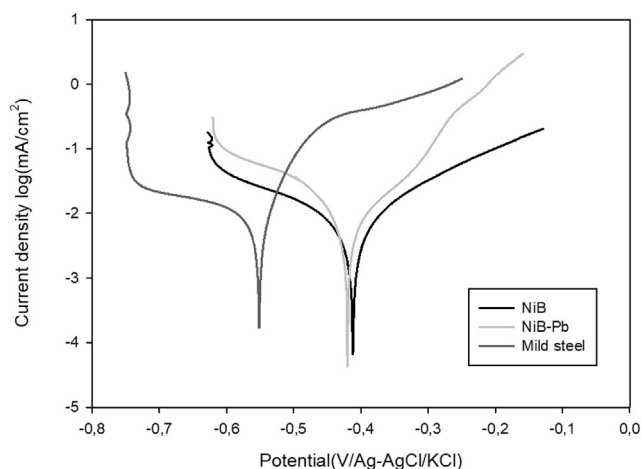


Fig. 7. Potentiodynamic polarization curves, 0.1 M NaCl, mild steel, electroless NiB and electroless NiB-Pb.

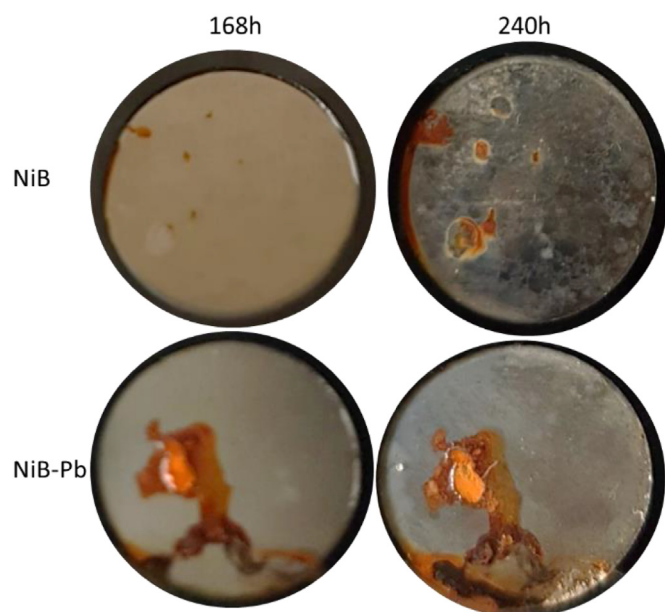


Fig. 8. Surface aspect of electroless NiB and NiB-Pb $15 \pm 1 \mu\text{m}$ coatings after 168 h and 240 h salt spray testing.

started to corrode, while the corrosion of NiB coatings started just after 96 h. Concerning the bare mild steel, corrosion started after 1 h and the surface was completely corroded after 8 h [42]. The aspect of the coated samples after 168 and 240 h of salt spray exposure is shown in Fig. 8. After 7 days (168 h) in neutral salt spray, the NiB samples presented only 0.8% of its surface corroded and this value increased to 3.6% after 240 h. After the same periods of testing, the NiB-Pb coatings presented 18.0 and 21.2% of corroded surface, respectively. The difference in the results obtained for both systems is in accordance with the polarization tests. Furthermore, they highlight the increase of the barrier properties of the NiB coatings when compared with the NiB-Pb system. The corrosion initiation time and the percentage of corroded surface are affected by the surface conditions, which explains the fact that smoother samples absent in columns present a better corrosion behavior.

5. Conclusion

Electroless NiB coating was developed by a completely new bath

free of stabilizer. The same equipment and conditions employed for obtaining traditional NiB coatings were considered. The composition of these new coatings comprises only Ni and B, thus not presenting co-deposition of heavy metals, which constitutes an essential aspect for the recyclability of Ni-B coatings. The plating bath without added stabilizer was optimized using an experimental design approach. In order to provide a coating thickness in a range of 10.0–10.6 μm (in one hour) and a roughness ranging between 0.22 and 0.25 μm , it was found that the concentrations of ethylenediamine and sodium hydroxide should stay between 120.0 and 128.7 g L^{-1} , and 151.7 and 160.0 g L^{-1} , respectively. The adjustment of pH using higher concentrations of sodium hydroxide was found to improve the coating thickness, while the decrease of ethylenediamine was found to reduce the roughness of the film.

The optimized NiB bath mixture consisted of 120 g L^{-1} of ethylenediamine and 160 g L^{-1} of sodium hydroxide, in the absence of lead, nor thallium nor other stabilizers. The resulting coatings, when compared with reference coatings obtained with a conventional bath (NiB-Pb), showed modified chemical composition and presented different growth mode, morphology, mechanical, tribology and corrosion behavior. Changes in the cross section morphology were also observed, as the new coatings present a featureless cross section due to the new growth mode. The surface morphology of the coatings did not present the cauliflower-like surface texture generally presented by electroless nickel boron coatings. Furthermore, the coatings presented an increase in the boron concentration that ensured a low friction coefficient in a flat surface. Regarding the mechanical properties, the new coatings presented quite interesting values of roughness (0.2 μm) and stabilizers showed to have an influence on the high hardness of NiB-Pb coatings. The most promising results obtained were related to the corrosion behavior, as the new coatings generated an efficient barrier between the environment and the protected steel.

Acknowledgments

The authors would like to thank Mr Enrique Juste from BCRC (Mons, Belgium) for his help with the realization of the scratch experiments. In addition, the authors would like to thank Dr. Sofia Gaiaschi from HORIBA Scientific (Palaiseau, France) for his help with the realization of the GDOES analyses. L. Bonin thanks as well the CNPq (Conselho Nacional de Desenvolvimento Científico e Tecnológico) for funding.

Appendices

Table A1

Results of the Standard least squares analysis - Effect of the ethylenediamine and sodium hydroxide in the coating thickness. * Results statistically significant. ** Results with no statistical relevance (more experiments needed).

Term	Coefficient	t-value	p-value
Ethylenediamine	0.813	3.430	0.0140**
Sodium hydroxide	1.295	5.460	0.0016*
Ethylenediamine * Sodium hydroxide	-0.170	-0.720	0.500

Table A2

Results of the Standard least squares analysis - Effect of the ethylenediamine and sodium hydroxide in the coating roughness. * Results statistically significant.

Term	Coefficient	t-value	p-value
Ethylenediamine	0.065	7.970	0.0002*
Sodium hydroxide	0.010	1.230	0.2659
Ethylenediamine * Sodium hydroxide	0.012	1.530	0.1761

References

- [1] P. Peelers, G.V.D. Hoorn, T. Daenen, A. Kurowski, G. Staikov, Properties of electroless and electroplated Ni-P and its application in microgalvanics, *Electrochim. Acta* 47 (2001) 161–169, [https://doi.org/10.1016/S0013-4686\(01\)00546-1](https://doi.org/10.1016/S0013-4686(01)00546-1).
- [2] S. Djokic, *Modern Aspects of Electrochemistry*, Mordechay, Edmonton, AB, Canada, 2014, <https://doi.org/10.1007/978-1-4939-0289-7>.
- [3] W. Riedel, *Electroless Nickel Plating Riedel, W ASM International: Metals Park, OH; 1991, ASTM International, Metals Park, OH, 1991*.
- [4] B. Zhang, Mechanism of electroless plating, in: Chemical Industry Press (Ed.), *Amorph. Nano Alloy. Electroless Depos.*, Elsevier Inc., Amsterdam, Netherlands, 2016, pp. 583–627, <https://doi.org/10.1016/B978-0-12-802685-4.00010-8>.
- [5] B.N.G. K. I. Popov, S.S.Djokic, Metal deposition without an external current, in: Kluwer academic publishers, New York, n.d.
- [6] M. Schliesinger, Electroless deposition of nickel, in: M.P. Mordechay Schlesinger (Ed.), *Mod. Electroplat.*, fifth ed., The electrochemical society series, 2010 <https://doi.org/10.1149/1.2425993>.
- [7] W.H. Safranek, Electroless cobalt and cobalt alloys section, in: J.B.H. Glenn, O. Mallory (Eds.), *American Electroplaters and Surface Finishing Society, New York, 1990*, pp. 463–509.
- [8] G.O. Mallory, The fundamental aspects of electroless nickel plating, in: *Electroless Plat. - Fundamentals Appl.*, American electroplaters and surface finishing society, New York, 1990, pp. 1–56.
- [9] M. Sribalaji, P. Arunkumar, K.S. Babu, A.K. Keshri, Crystallization mechanism and corrosion property of electroless nickel phosphorus coating during intermediate temperature oxidation, *Appl. Surf. Sci.* 355 (2015) 112–120, <https://doi.org/10.1016/j.apsusc.2015.07.061>.
- [10] R. Hu, Y. Su, H. Liu, Deposition behaviour of nickel phosphorus coating on magnesium alloy in a weak corrosive electroless nickel plating bath, *J. Alloys Compd.* 658 (2016) 555–560, <https://doi.org/10.1016/j.jallcom.2015.10.300>.
- [11] Y. Gan, D. Chen, Z. Kang, A highly anticorrosive chromium-free conversion coating prepared on electroless Ni – P coating, *Surf. Coating. Technol.* 287 (2016) 25–32, <https://doi.org/10.1016/j.surfcoat.2015.12.080>.
- [12] F. Madah, A.A. Amadeh, C. Dehghanian, Investigation on the phase transformation of electroless Ni-B coating after dry sliding against alumina ball, *J. Alloys Compd.* 658 (2016) 272–279, <https://doi.org/10.1016/j.jallcom.2015.10.156>.
- [13] Y. Wan, Y. Yu, L. Cao, M. Zhang, J. Gao, C. Qi, Corrosion and tribological performance of PTFE-coated electroless nickel boron coatings, *Surf. Coating. Technol.* 307 (2016) 316–323, <http://doi.org/10.1016/j.surfcoat.2016.09.001>.
- [14] C.A. Garcia-Aguirre, C. Dominguez-Rios, R. Torres-Sanchez, M. Roman-Aguirre, J.T. Holguin-Momaca, A. Aguilar-Elguezabal, Microstructure and transmission electron microscopy characterization of electroless Ni-B thin films deposited on MWCNTs, *Surf. Coating. Technol.* 282 (2015) 107–114, <https://doi.org/10.1016/j.surfcoat.2015.10.023>.
- [15] W.J. Cheong, B.L. Luan, D.W. Shoesmith, The effects of stabilizers on the bath stability of electroless Ni deposition and the deposit, *Appl. Surf. Sci.* 229 (2004) 282–300, <https://doi.org/10.1016/j.apsusc.2004.02.003>.
- [16] I. Baskaran, T.S.N.S. Narayanan, A. Stephen, Effect of accelerators and stabilizers on the formation and characteristics of electroless Ni-P deposits, *Mater. Chem. Phys.* 99 (2006) 117–126, <https://doi.org/10.1016/j.matchemphys.2005.10.001>.
- [17] X. Yin, L. Hong, B. Chen, Role of a Pb 2 + stabilizer in the electroless nickel plating System: a theoretical exploration, *J. Phys. Chem. B* (2004) 10919–10929, <https://doi.org/10.1021/jp036070k>.
- [18] B. Zhang, Impact parameters and deposition rate, in: *Amorph. Nano Alloy. Electroless Depos.*, Elsevier Inc., 2016, <https://doi.org/10.1016/B978-0-12-802685-4/00006-6>.
- [19] G.O. Mallory, The electroless nickel plating bath: effect of variables on the process, in: *Electroless Plating, Fundam. Appl.*, vol. 69, 2009, pp. 62–72.
- [20] C.E. McComas, Corrosion/wear-resistant Metal Alloy Coating Compositions, 1991. US5019163A.
- [21] I.N. Feldstein, *Surface Technology, Stabilizer for Composite Electroless Plating, 2001. US6306466B1*.
- [22] K. Parker, *Process of Electrolessly Depositing, Metal Coating Having Metallic Particles Dispersed Therethrough, 1971. US3562000A*.
- [23] C. Edward McComas, *Nodular Nickel Boron Coating, US2004229068A1, 2004*.
- [24] A. Mukhopadhyay, T.K. Barman, Effects of heat treatment on tribological behavior of electroless Ni – B coating at elevated temperatures, *Surf. Rev. Lett.* 25 (2018) 1–22, <https://doi.org/10.1142/S0218625X18500142>.
- [25] L. Bonin, N. Bains, V. Vitry, A.J. Cobley, Electroless deposition of nickel-boron coatings using low frequency ultrasonic agitation: effect of ultrasonic frequency on the coatings 77 (2017) 61–68, <https://doi.org/10.1016/j.ultras.2017.01.021>.
- [26] K.L. Lin, J.W. Hwang, Effect of thiourea and lead acetate on the deposition of electroless nickel, *Mater. Chem. Phys.* 76 (2002) 204–211, [https://doi.org/10.1016/S0254-0584\(01\)00516-8](https://doi.org/10.1016/S0254-0584(01)00516-8).
- [27] Council of the European Union, DIRECTIVE 2002/95/EC OF THE EUROPEAN PARLIAMENT AND OF THE COUNCIL of 27 January 2003 on the restriction of the use of certain hazardous substances in electrical and electronic equipment, *Off. J. Eur. Union. L 37/19* (2003), <https://doi.org/10.1016/j.jclepro.2010.02.014>.
- [28] EC, Directive 2000/53/EC of the European parliament and of the council of 18 september 2000 on end-of-life vehicles, *Eur. Comm.* 2137 (2000), 010.001-1-010.001-22, <http://ec.europa.eu/environment/waste/elvj/>.
- [29] EU, Directive 2012/19/EU of the European Parliament and of the Council of 4 July 2012 on Waste Electrical and Electronic Equipment, 2012, <https://doi.org/10.3000/19770677.L.2012.197.eng>.
- [30] P. Sahoo, S.K. Das, Tribology of electroless nickel coatings - a review, *Mater. Des.* 32 (2011) 1760–1775, <https://doi.org/10.1016/j.matdes.2010.11.013>.
- [31] V. Group, *Chemical Substances Which Must Not Be Present in Processes or Products within the Volvo Group, 2017*.
- [32] Y.S. Huang, F.Z. Cui, Effect of complexing agent on the morphology and microstructure of electroless deposited Ni-P alloy, *Surf. Coating. Technol.* 201 (2007) 5416–5418, <https://doi.org/10.1016/j.surfcoat.2006.07.189>.
- [33] W. Ke, *Development of Lead-free Electroless Nickel Plating Systems and Metal Thin Films on Silicone and Nafion Membranes*, National University of Singapore, 2008.
- [34] J. Kivrel, J.S. Sallo, The effect of thiourea on alkaline electroless deposition, *J. Electrochem. Soc.* (1965) 1201–1203, <https://doi.org/10.1149/1.2423399>.
- [36] N.G. Tsierekzos, D. Schröder, H. Schwarz, Complexation of nickel(II) by ethylenediamine investigated by means of electrospray ionization mass spectrometry, *Int. J. Mass Spectrom.* 235 (2004) 33–42, <https://doi.org/10.1016/j.ijms.2004.03.005>.
- [37] J. Guo, Y. Hou, C. Yang, Y. Wang, L. Wang, Effects of nickel ethylenediamine complex on the preparation of Ni-B amorphous alloy catalyst with ultrasonic assistance, *Mater. Lett.* 67 (2012) 151–153, <https://doi.org/10.1016/j.matlet.2011.09.059>.
- [38] B. Hu, R. Sun, G. Yu, L. Liu, Z. Xie, X. He, X. Zhang, Effect of bath pH and stabilizer on electroless nickel plating of magnesium alloys, *Surf. Coating. Technol.* 228 (2013) 84–91, <https://doi.org/10.1016/j.surfcoat.2013.04.011>.
- [39] L.B.V. Vitry, Formation and characterization of multilayers borohydride and hipophosphite reduced electroless nickel deposits, *Electrochim. Acta* 243 (2017) 7–17, [https://doi.org/10.1016/S0925-8388\(03\)00680-7](https://doi.org/10.1016/S0925-8388(03)00680-7).
- [40] V. Vitry, A. Sens, F. Delaunois, Comparison of various electroless nickel coatings on steel: structure, hardness and abrasion resistance, *Mater. Sci. Forum* 783–786 (2014) 1405–1413, <https://doi.org/10.4028/www.scientific.net/MSF.783-786.1405>.
- [41] K. Krishnaveni, T.S.N.S. Narayanan, S.K. Seshadri, Corrosion resistance of electrodeposited Ni-B and Ni-B-Si3N4 composite coatings, *J. Alloys Compd.* 480 (2009) 765–770, <https://doi.org/10.1016/j.jallcom.2009.02.053>.
- [42] L. Bonin, V. Vitry, F. Delaunois, Corrosion behaviour of electroless high boron-nitride phosphorous nickel duplex coatings in the as-plated and heat-treated states in NaCl, H2SO4, NaOH and Na2SO4 media, *Mater. Chem. Phys.* 208 (2018) 77–84, <https://doi.org/10.1016/j.matchemphys.2017.12.030>.